ACS OMEGA

http://pubs.acs.org/journal/acsodf

Article

Fe-Based Metal–Organic Frameworks for the Controlled Release of Fertilizer Nutrients

Ke Wu, Xuebin Xu, Fei Ma, and Changwen Du*

Cite This: *ACS Omega* 2022, 7, 35970−35980

Read Online

ACCESS | Metrics & More | Article Recommendations | Supporting Information

ABSTRACT: Due to the controlled-delivery function of metal−organic frameworks (MOFs) for gases, drugs, and pesticides, iron-based MOFs (Fe-MOFs) were explored in the laboratory as a novel fertilizer, which showed potential for use in the fertilizer industry; the challenge in the industrial scale application of Fe-MOFs in practical crop production was mainly the impact of scaling-up to energy and heat transfer, as well as the reaction yield. In this study, Fe-MOFs were hydrothermally synthesized both in the laboratory scale and in the pilot scale, their structure and components were characterized using various spectroscopic techniques, and then their nutrient release and degradation behaviors were investigated.

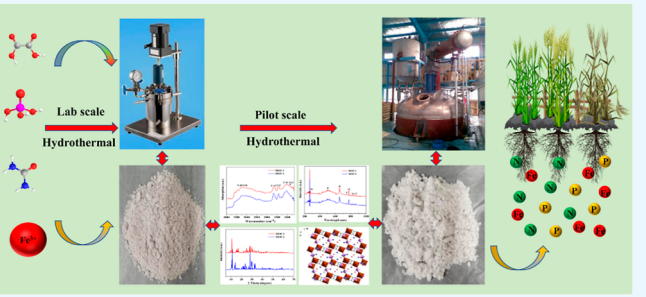

The results showed that Fe-MOFs were successfully synthesized in both scales with similar yields around 27%, and the Fe-MOFs showed a similar structure with the molecular formula of $C_2H_{15}Fe_2N_2O_{18}P_3$. The nutrients N, P, and Fe were present in the Fe-MOFs with the average contents of 6.03, 14.48, and 14.69%, respectively. Importantly, the nutrient release rate and pattern of Fe-MOFs well matched with the crop growth, which greatly promoted the rice yield. Therefore, the environmentally friendly compounds of Fe-MOFs could be industrially produced and used as an innovative fertilizer with unique features of varied nutrients and controlled release.

INTRODUCTION

The low-nutrient utilization rate of conventional fertilizers resulted in serious non-point source pollution, which has inspired extensive efforts in the research and development of controlled-release fertilizers over the past 2 decades. Currently, controlled-release fertilizers using petroleum-based polymers (polyethylene, polyurethane, etc.) as coating materials have revolutionized agriculture and have become quite popular. However, the non-renewability and high price of these coating materials limited its application in a large scale.[1,2] What is more, fertilizer-containing plastic microcapsules with a diameter of 2−5 mm ("coated fertilizer") are not recovered after use of these materials, resulting in the accumulation and excess of microcapsules in soil, which pose serious environmental risks.[3] Controlled-release fertilizers prepared from starch,[4] lignin and cellulose,[5,6] chitosan,[7] alginate,[8] and other bio-based coating materials were environmentally friendly; however, their release nutrient rates were too fast (<30 d) due to low hydrophobicity of the coating materials, which led to a problem in the nutrient match with crop growth. Therefore, metal−organic framework (MOF) compounds provide a novel option for the development of low-cost, environmental-friendly, controlled-release fertilizers.

MOFs are functional materials self-assembled by metal ions or ion clusters and organic ligands. These materials have realized controllable design and synthesis at the molecular level. MOF materials with specific structures and functions are constructed by pre-directional topology design, making full use of specific organic ligand orientations during coordination. Compared to traditional inorganic and organic materials, MOF materials possess advantages such as large specific surface areas,[9] high porosities,[10] diverse configurations,[11] and adjustable structures.[12] MOF materials have been extensively used in the fields of gas storage and separation,[13,14] catalysis,[15] fluorescent probes,[16−18] and drug carriers.[19]

In agriculture, there have been reports on utilizing MOF materials as fertilizers. Abdelhameed et al. investigated the effect of iron-based MOF (Fe-MOF)−EDTA as an iron fertilizer and found that the MOF significantly improved the biomass, chlorophyll content, and enzyme activity of kidney beans.[20] Anstoetz et al. reported an oxalate-phosphate amine-MOF (OPA-MOF) material that contained nitrogen, phosphorus, and iron nutrients, and a pot culture experiment showed this MOF material significantly improved the wheat yield and nitrogen utilization efficiency, which indicated that the OPA-MOF had potential as a synergistic nitrogen

Received: August 9, 2022
Accepted: September 21, 2022
Published: September 30, 2022

fertilizer.[21] Wu et al. hydrothermally synthesized an MOF with a high nitrogen load, and soil culture results showed that this material exhibited good controlled-release effect on nutrients.[22] In addition, there were also reports on MOF synthesis under solvent-free conditions and its application as a slow-release fertilizer.[23] Previous studies have demonstrated that MOF materials have great potential and broad application prospects as a slow-/controlled-release fertilizer. However, the investigations were limited in the laboratory scale, and pilot-scale production of MOF materials as fertilizers has not been conducted yet. Due to differences in raw material sources, reactor materials, heat transfer, and stirring methods, pilot-scale production of MOF materials should differ from laboratory products, and it is necessary to explore the pilot-scale production of MOF prior to industrial production as a fertilizer.

The objectives of this study were to (1) hydrothermally synthesize a Fe-MOF rich in nitrogen, phosphorus, and iron using water as the substrate in the pilot scale, (2) characterize the structure and components of the synthesized Fe-MOF, (3) explore the nutrient controlled-release performance and degradation behaviors of the synthesized Fe-MOF and then evaluate its potential as a controlled-release fertilizer, which provided support for the industrial production. As a result, by comparing the similarities and differences in the structure and function of Fe-MOFs synthesized in the pilot scale and laboratory scale, the synthesis process conditions were adjusted and optimized.

EXPERIMENTAL SECTION

Materials. Ferric chloride ($FeCl_3{\cdot}6H_2O$), oxalic acid ($H_2C_2O_4{\cdot}2H_2O$), urea ($CO(NH_2)_2$), and phosphoric acid (H_3PO_4) were purchased from Nanjing Ronghua Scientific Equipment Co., Ltd. (Jiangsu, China). All reagents mentioned above are of both industrial grade and analytical grade. Process water and deionized water were used throughout the pilot-scale and laboratory-scale experiments, respectively. Apparatuses for preparing Fe-MOFs were a hydrothermal reactor (3000L) (Yangzhou Tongyang Chemical Equipment Co. Ltd., China) and a KCF-2 autoclave (3L) (Beijing Century Senlang Experimental Apparatus Co., China).

Synthesis of Fe-MOFs. *Pilot Scale (MOF1).* 150.16 kg of ferric chloride ($FeCl_3{\cdot}6H_2O$), 70 kg of oxalic acid ($H_2C_2O_4{\cdot}2H_2O$), 83 kg of urea ($CO(NH_2)_2$), 205.5 L of phosphoric acid (H_3PO_4), and 1000 L of process water were added to a hydrothermal reactor (3000 L) (Yangzhou Tongyang Chemical Equipment Co. Ltd., China), stirring constantly until all substrates were mixed evenly. The mixture was held at 100 °C for 24 h with the stirring speed set to 90 rpm. The resulting product was washed three times with deionized water and subsequently dried at 60 °C. The yield of Fe-MOFs was calculated by the following equation

$$\text{yield}\ (\%) = (\text{mass of Fe} - \text{MOFs}) / [\text{mass of substrates (ferric chloride, oxalic acid, urea and phosphoric acid)}] \times 100\% \quad (1)$$

Laboratory Scale (MOF2). The substrate used consisted of 67.5 g of ferric chloride, 31.5 g of oxalic acid, 37.3 g of urea, 92.4 mL of phosphoric acid, and 450 mL of deionized water. The dissolved and mixed substrates were transferred to the reactor KCF-2 autoclave (3 L) (Beijing Century Senlang Experimental Apparatus Co., China). The procedure was the same as that for MOF1.

For comparison, the Fe-MOF (MOF0) was synthesized. The synthetic procedure was carried out as that of MOF1, except that urea [$CO(NH_2)_2$] and phosphoric acid (H_3PO_4) were not added.

Fe-MOF Characterizations. The Fourier transform infrared attenuated total reflectance spectra (FTIR-ATR) of MOFs were recorded using a portable FTIR spectrometer (TurDefender FT, Thermo Fisher Scientific, USA) in the range of 4000−400 cm^{-1} at 4 cm^{-1} resolution. The Fourier transform infrared photoacoustic spectra (FTIR-PAS) of MOFs samples were acquired in the laboratory over the mid-infrared range (4,000−400 cm^{-1}) at 8 cm-1 resolution using an infrared spectrophotometer (Nicolet 6700, Themo-Scientific, USA), equipped with a photoacoustic detector (Model 300, MTEC, USA), the mirror velocity was set to 0.32 cm s^{-1} for spectra collections, and black carbon was used as reference. Powder X-ray diffraction (XRD) data were collected in the 3−70° range by an ARL X'TRA diffractometer (Thermo Electron Corporation, Switzerland) using a CuKα radiation source at 0.02° step size and 5° min^{-1} scanning rate, and the powder XRD data of MOF was compared to the International Centre for Diffraction Data (ICDD) for phase identification. A regular, transparent, crack-free crystal was extracted from the precipitate using tweezers under an optical microscope for single-crystal determination. Single-crystal XRD data were recorded using a D8Quest diffractometer (Bruker, Billerica, MA, USA) at 273 K. Data collection was carried out using the BluIce software suite with processing undertaken in the XDS program. Analyses and refinements of the crystal structures were carried out using a direct method with the help of SHELXTL software. The detailed information for microstructure, morphology, and surface topology of the Fe-MOFs were observed using scanning electron microscopy (SEM) (ZEISS Merlin 132 Compact, Germany) on 10 kV accelerating voltage (AV). The surface elemental compositions and distribution were analyzed using an energy-dispersive X-ray spectroscopy (EDX) detector attached to a scanning electron microscope. The contents of C, N, and H of the Fe-MOFs were determined by an elemental analyzer (Vario EL cube, Elementar, Germany). The compounds were completely dissolved with HCl (6 mol L^{-1}), and P and Fe were determined by inductively coupled plasma optical emission spectrometry (ICP−OES) (Thermo Fisher Scientific, USA). Laser-induced breakdown spectrometry (LIBS) (IVEA, France) utilizing the AnaLIBS control software was performed to obtain the LIBS spectra of MOF samples. The laser beam with 532 nm and 5 ns pulse duration was generated from a fourth-harmonic Nd:YAG laser (Quantel, France). The frequency of the system was 20 Hz, and the delivery energy was 16 mJ. The laser beam was focused on the soil tablet samples to form a spot with 50 μm diameter using a lens with 15 cm focal length. The emission line of the resulting plasma was transmitted from a light collector to the Mechelle ME5000 Echelle spectrograph (Andor Technology, Ltd., Northern Ireland). The resolving power of this spectrograph was $\lambda/\Delta\lambda$ = 4000. An intensified charge-coupled device camera (iStar, Andor Technology, Ltd., Northern Ireland) collected the diffracted light to generate the LIBS spectrum. The delay time and the gate width were controlled and set to be 370 μs and 7.0 ms, respectively. The wavelength range was 200−1000 nm,

https://doi.org/10.1021/acsomega.2c05093
ACS Omega 2022, 7, 35970−35980

and the spectral resolution was 0.116 nm. X-ray photoelectron spectroscopy (XPS) analysis of the samples was conducted (Escalab 250Xi, Thermo Fisher Scientific, UK) using monochromatized Al-KD radiation (1486.6 eV; energy step size: 0.050 eV). The binding energy scale was calibrated with respect to the C1s signal at 284.8 eV.

Nutrient Release Behaviors from Fe-MOFs. *Nutrient Release in Water.* 3 g of each Fe-MOF sample was placed in a 250 mL glass bottle containing 200 mL of deionized water at 25 °C (with three replicates). The nutrient release rate was measured at 1, 3, 5, 7, 14, 21, 28, 35, 42, 56, 70, 84, and 98 d, respectively. The NH_4^+-N and NO_3^--N contents were determined using a SmartChem 200 discrete auto analyzer, while the urea content was determined by the *para*-dimethylamino-benzaldehyde colorimetric method. The total P and Fe contents were analyzed by an ICP-OES system (iCAP 7000, Thermo Fisher Scientific, Waltham, MA, USA). The pH values of the water solutions were determined using an Orion Star A211 pH meter. The nutrient release behaviors were estimated via nutrient cumulative release rates.

Nutrient Release in Soil. Soil incubation experiments were conducted to further investigate the nutrient release behaviors of MOF using paddy soil (air-dried and sieved to 3 mm). The soil physicochemical properties were as follows: organic matter, 19.76 g kg^{-1}; total N, 1.32 g kg^{-1}; NH_4^+-N, 11.35 mg kg^{-1}; NO_3^--N, 13.21 mg kg^{-1}; available P, 16.88 mg kg^{-1}; available K, 177.5 mg kg^{-1}; and available Fe, 6.81 g kg^{-1}; pH, 6.43. Three treatments were prepared: (1) control treatment and (2) MOF1 treatment. 200 g of soil sample was placed in 8 cm diameter pots, 2.5 g of MOF sample wrapped in a gauze with an aperture of 74 μm was buried in soil, and the moisture was adjusted to 38% (w/w). (3) MOF2 treatment. The procedure was the same as that for MOF1. A total of 117 pots (39 pots per treatment) were prepared. All the pots were placed in a shade house and were loosely covered with a plastic wrap to reduce soil water evaporation. The soil and Fe-MOF samples were collected at 1, 3, 5, 7, 14, 21, 28, 35, 42, 56, 70, 84, and 98 d. All soil and Fe-MOF samples were air-dried.

The mineral N (NH_4^+-N and NO_3^--N) contents were determined by a SmartChem 200 discrete auto analyzer. An ICP-OES spectrometer was used to measure the soil available P and Fe. The soil pH was measured using an Orion Star A211 pH meter. The N, P, and Fe release rates from the Fe-MOFs were estimated by the mineral N, available P, and available Fe in the soil. The calculation formulas were as follows

$$\begin{aligned}&\text{ineral N cumulative release rate\(\%)}\\&= (\text{mass of } NH_4^+ - \text{N and } NO_3^- - \text{N released from Fe}\\&\quad - \text{MOFs})/(\text{mass of N in Fe} - \text{MOFs}) \times 100\% \end{aligned} \quad (2)$$

$$\begin{aligned}&\text{vailable P cumulative release rate (\%)}\\&= (\text{mass of available P released from Fe} - \text{MOFs})\\&\quad /(\text{mass of P in Fe} - \text{MOFs}) \times 100\% \end{aligned} \quad (3)$$

$$\begin{aligned}&\text{vailable Fe cumulative release rate (\%)}\\&= (\text{mass of available Fe released from Fe} - \text{MOFs})\\&\quad /(\text{mass of Fe in Fe} - \text{MOFs}) \times 100\% \end{aligned} \quad (4)$$

The cumulative release data were assessed with the zero-order, first-order, Higuchi, and Ritger-Peppas models by eqs 5−8, respectively.[24−26]

Zero-order release kinetics model

$$M_t/M_\infty = kt \quad (5)$$

First-order release kinetics model

$$M_t/M_\infty = 1 - e^{kt} \quad (6)$$

Higuchi model

$$M_t/M_\infty = kt^{0.5} \quad (7)$$

Ritger-Peppas model

$$M_t/M_\infty = kt^n \quad (8)$$

where M_t/M_∞ is the nitrogen release rate (%) at time t, k is the rate constant, and n is the diffusion parameter. The release mechanism is classified by the diffusion index (n). If $n < 0.43$, it is the Fickian diffusion mechanism; if $0.43 < n < 0.85$, it belongs to the non-Fickian diffusion mechanism; and if $n > 0.85$, it belongs to Case-II transport.[27]

Fe-MOF samples were weighed for calculation of the degradation rate. A Hitachi SU8200 scanning electron microscope, an FTIR-ATR spectrometer, and a LIBS system were used to analyze the structural changes of MOF during the incubation process.

Application of Fe-MOFs in Field Rice. *Experimental Materials.* Conventional fertilizer—urea (N 46%), potassium sulfate (K_2O 52%), and superphosphate (P_2O_5 12%); MOF pilot-scale controlled-release fertilizer—N 6.2%, P_2O_5 33.48%, Fe 13.83%; rice variety—Wuyunjing 23.

Field Site and Trial Design. The trial was conducted at the Tangquan Experimental Base of the Nanjing Institute of Soil Science, Chinese Academy of Sciences (32°04′ 15″N, 118°28′21″E). Soil physical and chemical properties are as follows: organic matter, 18.25 g·kg^{-1}; total nitrogen, 1.23 g·kg^{-1}; ammonium nitrogen, 12.15 mg·kg^{-1}; nitrate nitrogen, 14.33 mg·kg^{-1}; available phosphorus, 17.65 mg·kg^{-1}; available iron, 7.95 mg·kg^{-1}; pH, 6.58. The trial period: June 9, 2020 to November 15, 2020.

Experimental Treatments. (1) No fertilizer control (CK) and (2) conventional fertilization (CF). Fertilization levels were N, 150 kg·hm^{-2}; P_2O_5, 150 kg·hm^{-2}; and K_2O, 120 kg·hm^{-2}. Phosphorus and potassium fertilizers were applied as the base fertilizer, and the nitrogen fertilizer was applied as the base fertilizer, tillering fertilizer, and panicle fertilizer at a ratio of 5:2:3; and (3) Fe-MOF group. Fe-MOFs were used to replace some conventional fertilizers (20% replacement of conventional nitrogen, conventional phosphate fertilizer was not applied, and potassium fertilizer was applied as the base fertilizer at the same fertilization level as CF). Four replicate plots were set up for each treatment, and each experimental plot was 20 m^2 (4 m × 5 m). On June 9, 2020, rice seedlings with uniform size were artificially transplanted with a row spacing of 25 cm and a plant spacing of 20 cm. Normal field management was implemented during the experiment. Harvested on November 15, 2020, and the crop yields were tested.

Determination of Agronomic Traits of Rice. At the mature stage, a 1 m^2 quadrat was selected from each experimental plot to determine the agronomic traits of rice, including the 1000 kernel weight, seed setting rate, number of kernels per ear, and

https://doi.org/10.1021/acsomega.2c05093
ACS Omega 2022, 7, 35970−35980

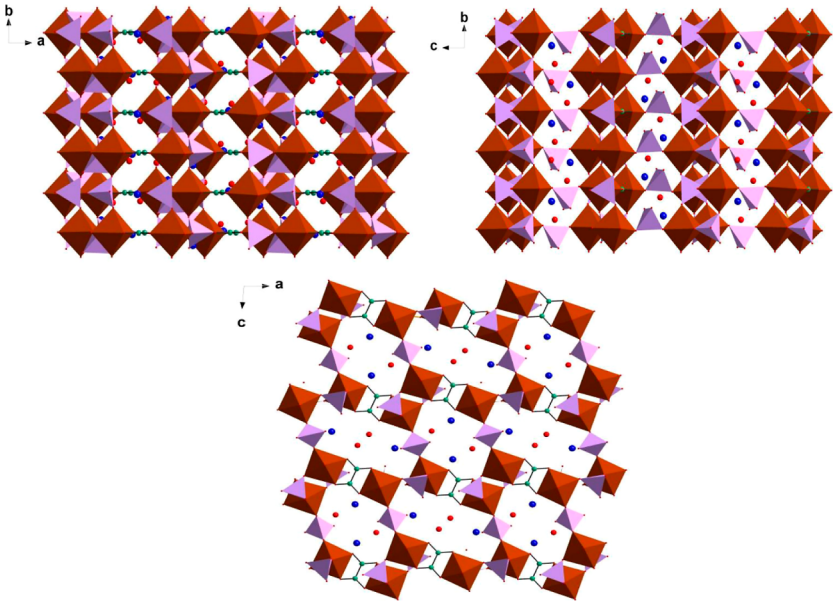

Figure 1. Crystal structure of Fe-MOFs. FeO_6 units are represented by red octahedra, PO_4 units by purple tetrahedra, NH_4^+ units by blue spheres, H_2O by red spheres, and C atoms by green spheres.

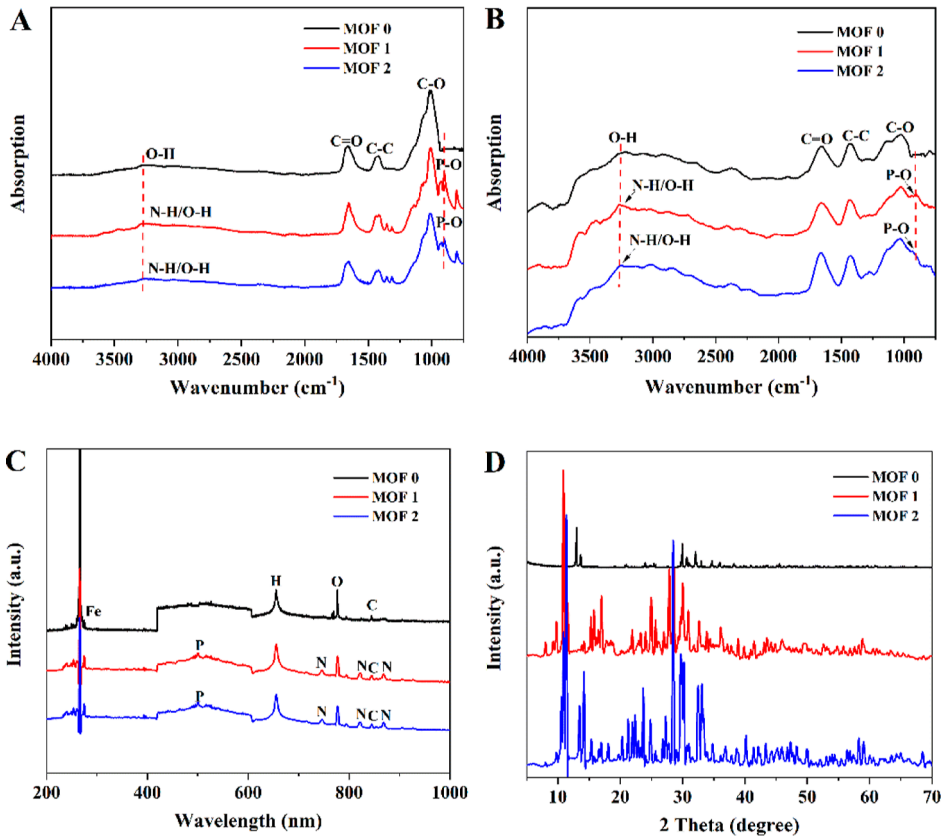

Figure 2. Structural characterizations of three Fe-MOFs by ATR-FTIR spectra (A), FTIR-PAS spectra (B), LIBS spectra (C), and PXRD (D).

number of effective ears. In addition, 20 plants were randomly selected from each plot; the plant samples were dried in an oven at 105 °C for 30 min and 80 °C at least for 72 h to achieve a constant weight, and the biomass and total nitrogen content of plant straw and rice ears were determined. The ground plant samples were digested with the H_2SO_4–H_2O_2 mixture, and the total nitrogen content was determined by a SmartChem200 automatic analyzer (Alliance, France). The plant nitrogen accumulation and nitrogen use efficiency were determined using the following equation

$$\text{plant nitrogen accumulation (N kg·hm}^{-2}) = \text{aboveground biomass (kg·hm}^{-2}) \times \text{plant nitrogen content (kg/kg)} \quad (9)$$

https://doi.org/10.1021/acsomega.2c05093
ACS Omega 2022, 7, 35970−35980

nitrogen use efficiency (%)

= [plant nitrogen absorption (Fe − MOF treatments) − plant nitrogen absorption (CK)]/ nitrogen rate × 100 (10)

Statistics and Data Analysis. Excel 2010 was used to organize and count the test data. Statistics and significant differences were determined using software SPSS 19.0 (SPSS, Inc., Chicago, IL, USA).

RESULTS AND DISCUSSION

Fe-MOF Characterizations. Single X-ray crystallographic analysis demonstrated that the crystallizes of MOF1 and MOF2 were in the monoclinic system with the same $P2_1/c$ space group (Table S1). It is a symmetric unit composed of two Fe^{3+} ions, one $C_2O_4^{2-}$ ligand, three PO_4^{3-} groups, two lattice water molecules, and two NH_4^+ groups (Figure 1). Fe was six-coordinated by four oxygen atoms from four PO_4^{3-} groups and two oxygen atoms from one $C_2O_4^{2-}$ ligand. Thus, the coordination geometry of Fe^{3+} was viewed as a slightly distorted octahedron. The Fe−O bond lengths ranged from 1.9159(16) to 2.1513(16) Å (Table S2). $C_2O_4^{2-}$ ligands adopt one coordination mode: carboxylate coordinated to two Fe^{3+}centers in a bis-bidentate mode. Each P atom was tetrahedrally coordinated by four O atoms with P−O bond lengths and O−P−O bond angles ranging from 1.4999 (18) to 1.5799(18) Å and 101.59(9) to 113.68(10) Å, respectively. In the Fe-MOFs, adjacent Fe^{3+} was bridged by two PO_4^{--} groups, forming an infinite ladder-like chain. These ladder-like chains formed a 2D layer by the linkage of PO_4^{3-} groups along the *bc* plane. Furthermore, the 2D layers were extended into a three-dimensional framework via the linkage of $C_2O_4^{2-}$ ligands. Two water molecules and two NH_4^+ groups were encapsulated in the cavities of the framework.

Figure 2A,B shows that both the MOF1 and MOF2 FTIR spectra were similar. The wide peak at 3250 cm^{-1} belongs to the stretching vibration of N−H/O−H. The characteristic bands at 1650, 1430, and 1025 cm^{-1} correspond to the stretching vibrations of C═O, C−C, and C−O, respectively, which confirmed the successful incorporation of an oxalic acid group. In the fingerprint region, the smaller characteristic peak at 900 cm^{-1} corresponded to the stretching vibration of P−O, while the peak did not appear in MOF0, which indicated that phosphoric acid also participated in the thermolysis and became part of MOF1 and MOF2 materials. The MOF elemental composition was studied by LIBS (Figure 2C). MOF1 and MOF2 showed the same characteristic peaks; the peaks at 274.6, 500.3, 844.8, 777.3, and 655.6 nm corresponded to Fe, P, C, O, and H bands, respectively, and the peaks at 746.8, 819.2, and 868.3 nm were attributed to N, which confirmed that the two MOFs took on the same elemental composition and demonstrated that all substrates were involved in the chemical reaction to form the MOFs. For MOF0, the characteristic peaks of N and P were not observed. Figure 2D shows the MOF PXRD spectrum, and the characteristic peaks of the three MOFs differed, which indicated some structural differences in the three crystals. Both MOF1 and MOF2 indicated high crystallinity (91 and 92%, respectively). A comparison with the International Centre for Diffraction Data yielded no MOF match; therefore; the synthesized MOFs were classified as a new material, and the PXRD pattern simulated using single-crystal data was not completely consistent with the experimental spectrum, indicating that MOF1 and MOF2 contained other phases in addition to $C_2H_{15}Fe_2N_2O_{18}P_3$ (Figure S1).

The elemental compositions of the three Fe-MOF samples were determined using a CHN−O-rapid elemental analyzer and an ICP-OES system. As shown in Table 1, the overall parameter indexes of MOF1 and MOF2 were relatively close, which indicated that all substrates participated in the chemical reaction of target MOF synthesis.

Table 1. Yields and Nutrient Contents of MOF0, MOF1, and MOF2[a]

%	MOF0 (%)	MOF1	MOF2
yields	23.70	27.53	26.65
N		6.21	5.85
P		14.62	14.33
Fe	21.85	13.85	15.52
C	8.73	5.23	6.87
H	6.32	5.32	4.89

[a]MOF0, MOF synthesized in the laboratory scale; MOF1, MOF synthesized in the pilot scale; MOF2, MOF synthesized in the laboratory scale.

The elemental composition of the MOFs was also studied by XPS, and the peaks at 724, 532, 402, 285, and 134 eV corresponded to the characteristic peaks of Fe $2p_{1/2}$, O 1s, N 1s, C 1s, and P 2p, respectively, which confirmed that ferric chloride, oxalic acid, urea, and phosphoric acid all reacted to form MOF1 (Figure 3A−F). The characteristic spectrum of MOF1 was deconvoluted to obtain high-resolution characteristic peaks to study the chemical bond configuration. Fe^{3+} (712 eV), Fe^{2+} (709.2 eV), and RO-Fe (533.2 eV) revealed the chemical bond structure, confirmed the mixed valent state of Fe in MOF1, and matched with previous reports.[28−30] However, the mixed valence state of Fe in the MOF lab scale was inconsistent with the single-crystal structure that contains only Fe^{3+}, which further indicates that the MOF1 contained substances of other phases. The peak at 401.98 eV belonged to NH_4^+, which indicated the urea decomposition during thermolysis.

As a structure directing reagent (SDA), urea played an important role in the structure and stability of the target product. For most amine SDAs (diamines, diaminopropane, and piperazines) in MOF syntheses, their structures usually remain unchanged and are embedded in the MOF framework as guest molecules. However, previous studies have shown that, in some cases, SDAs partially or fully decompose into a more stable secondary structure.[31−33] In addition, the O−C═O (290.38 eV), C−O (288.78 eV), C−O (286.18 eV), and C−C (284.68 eV) bonds in the spectrum indicated the successful introduction of oxalic acid. The peak at 133.7 eV belonged to P−O and confirmed that phosphoric acid was involved in MOF formation and is part of its framework. MOF2 has basically the same XPS spectral characteristics as MOF1 (Figure 3G−L), which indicated that the compounds synthesized in the pilot-scale took on the same elemental composition and valence bond structure as the laboratory-synthesized MOFs.

The surface morphologies of both MOFs were observed by SEM at different magnifications. Figure 4A shows a rough and uneven MOF1 surface, gathered with many massive, different-

https://doi.org/10.1021/acsomega.2c05093
ACS Omega 2022, 7, 35970−35980

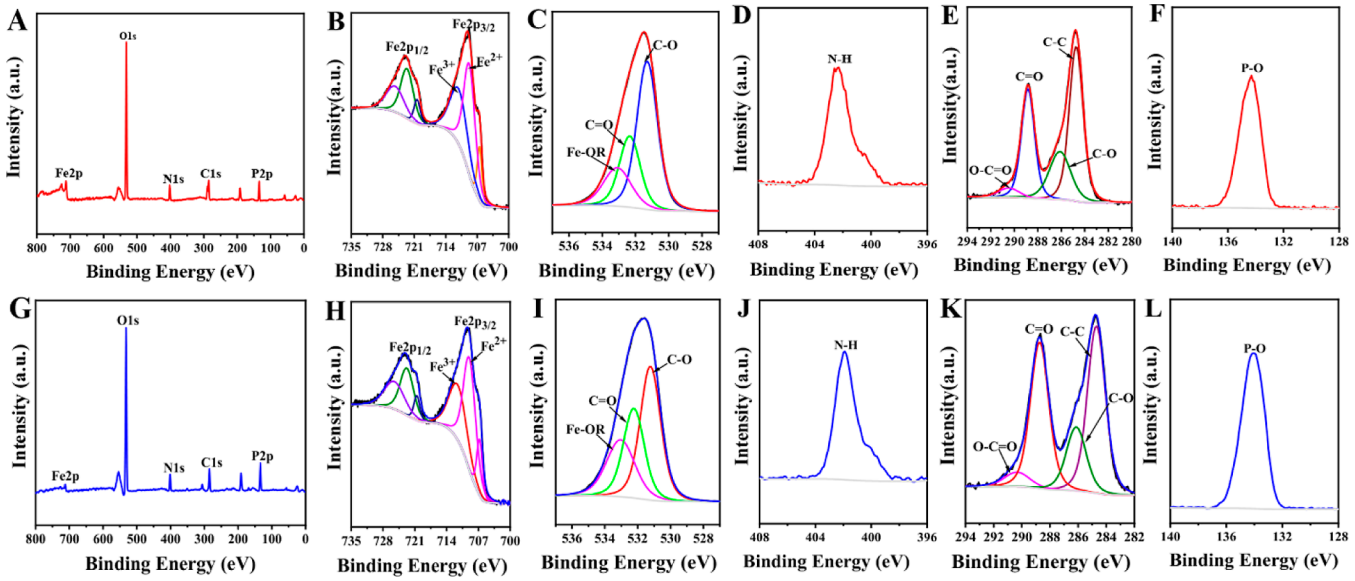

Figure 3. Elemental composition and the corresponding valence state on the surface of two Fe-MOFs. XPS spectra of MOF1 (A–F) and MOF2 (G–L).

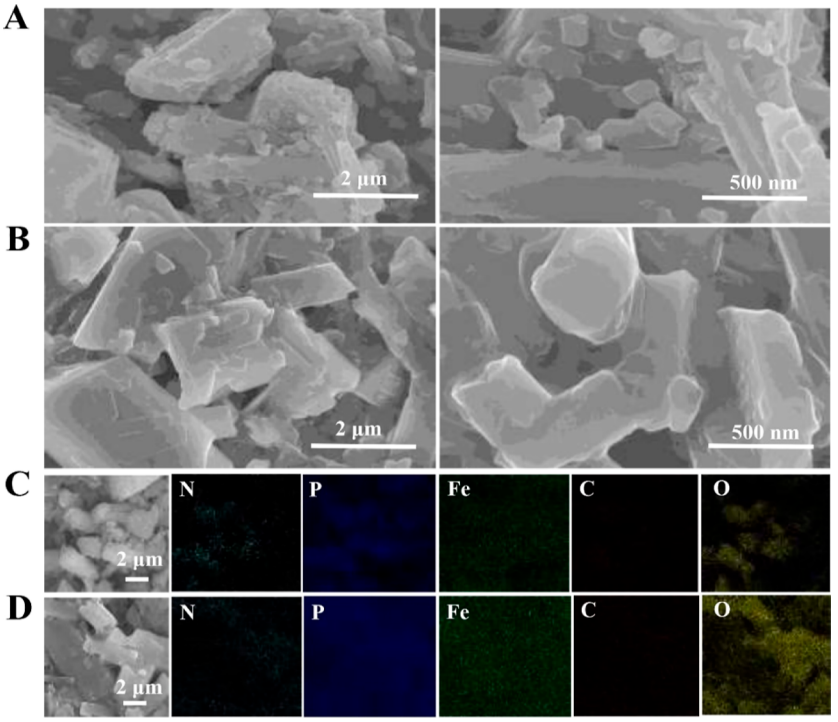

Figure 4. Microstructure and elemental distributions of two Fe-MOFs. SEM images of MOF1 (A) and MOF2 (B). EDX maps corresponding to the SEM images for surface elemental distributions of MOF1 (C) and MOF2 (D).

sized microcrystals, and similar to the MOF2 structure (Figure 4B). This indicated that products with similar surface structures were obtained upon scaling the hydrothermal reaction up from laboratory conditions. The EDX map observed the elemental surface composition and distribution of MOFs (Figure 4C,D). The EDX results not only confirmed the elemental composition obtained by FTIR-ATR, FTIR-PAS, LIBS, and XPS but also showed a better distribution of these elements. The figures show an even distribution of Fe, P, N, C, and O on the MOF surface and confirmed the participation of all reagents during the MOF synthesis.

Release Profiles of Nutrients from Fe-MOFs. To study the controlled-release ability of these materials, we measured the nutrient release rates in water at 25 °C. As shown in Figure 5A, MOF1 and MOF2 showed similar N release behaviors. The cumulative release rates of N within 98 days were 8.3 and 6.9%, respectively, far lower than the previously reported N release rates of coated slow-release fertilizers.[34,35] Interestingly, we found that almost all N in the aqueous solution came from urea, while urea and nitrate nitrogen were not detected, indicating that urea completely decomposed into ammonium nitrogen during thermolysis in agreement with XPS data. The

https://doi.org/10.1021/acsomega.2c05093
ACS Omega 2022, 7, 35970−35980

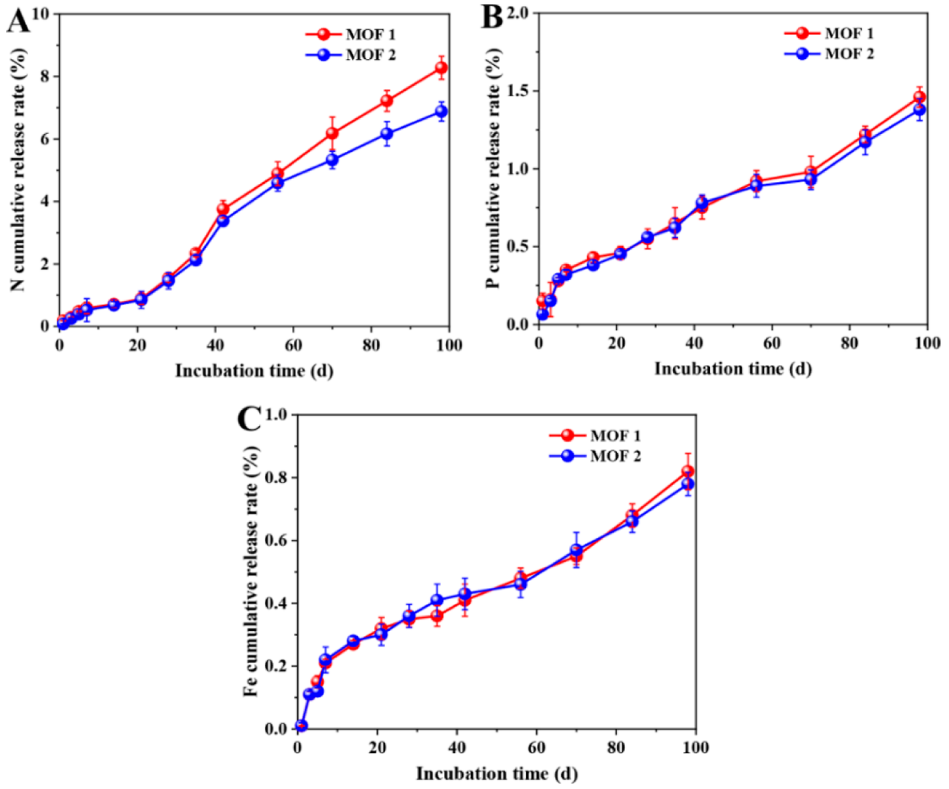

Figure 5. Nutrient release rates of two Fe-MOFs in water at 25 °C. (A) N cumulative release rate; (B) P cumulative release rate; and (C) Fe cumulative release rate.

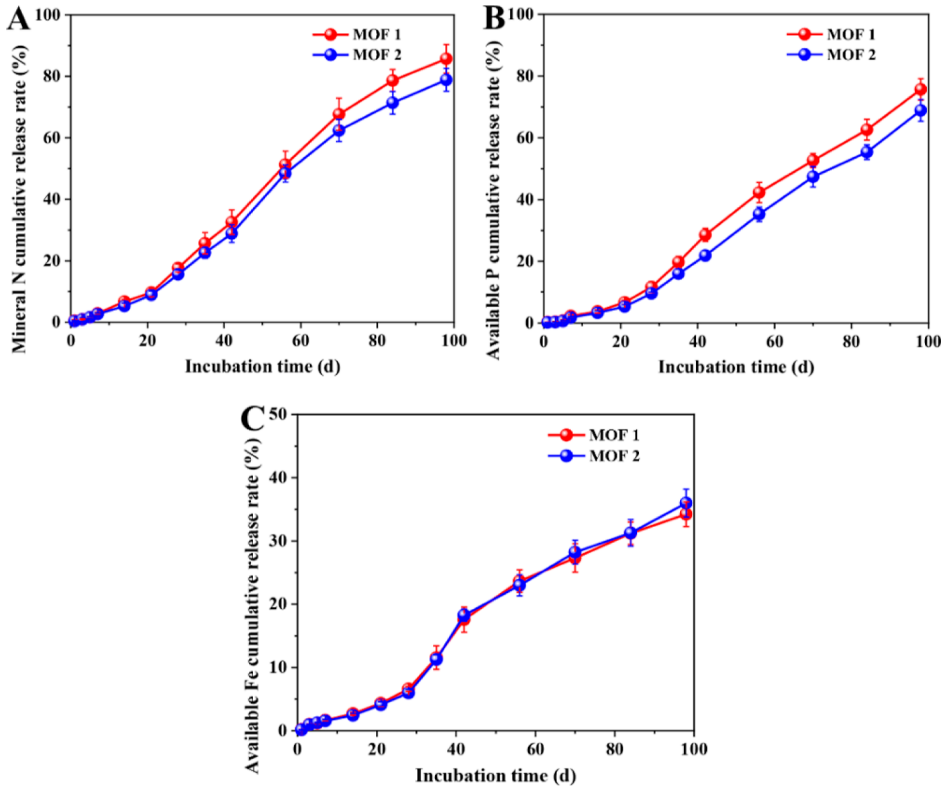

Figure 6. Nutrient release rates of two Fe-MOFs in soil. (A) Mineral N cumulative release rate. (B) Available P cumulative release rate. (C) Available Fe cumulative release rate.

cumulative release rates of P and Fe were lower than N (Figure 5B,C), likely due to the external localization of P and Fe on the MOF, while N was embedded in the pores inside the MOF framework in the form of ammonium nitrogen via a hydrogen

https://doi.org/10.1021/acsomega.2c05093
ACS Omega 2022, 7, 35970−35980

bond or van der Waals force.[36] Therefore, the release of P and Fe may be inhibited by the chemical bonds in the framework that resulted in a nutrient release lag. In addition, during the culture process, the pH of the water slowly decreased, possibly due to ammonium-ion hydrolysis. These results showed that MOF1 and MOF2 possess similar nutrient release behaviors. As we all know, the nutrient release characteristics of slow-/controlled-release fertilizers need to match the nutrient requirements of crops. However, the cumulative release rates of N, P, and Fe within 98 days of Fe-MOFs were all below 10%, which is far from meeting the growing needs of crops.

To truly understand the nutrient release law of MOFs, we conducted soil culture experiments. The nutrient release rates in soil for both MOFs arose significantly relative to water (Figures 5 and 6). The cumulative release rates within 98 days of mineral N from MOF1 and MOF2 were 85 and 78%, respectively, while the cumulative release rates of P were 75 and 68%, respectively, and for Fe they were 34 and 35%, respectively. Compared to N, the releases of P and Fe showed an obvious hysteresis, which agreed with their release behavior in water. The results certified that both MOFs showed similar nutrient release characteristics. Compared to NH_4^+ nitrification, Fe^{2+}/Fe^{3+} had a higher redox potential, so Fe^{2+} oxidation resulted in the release of two hydrogen ions from every Fe atom.[37] In this study, XPS results also showed mixed valent iron in the MOF. In conclusion, MOF favored nutrient release in soil relative to water, which can be attributed to the decomposition of the MOF by microorganisms in the soil. The oxalotrophic bacteria could consume the structurally incorporated oxalate in the MOF material, indicating that the microbially facilitated degradation of the MOF in the soil, thus resulting in a faster nutrient release from MOF.[38]

The release rates of N and P of MOF1 exceeded those of MOF2 and showed good features for use as a controlled-release fertilizer. The release mechanisms of N, P, and Fe from Fe-MOFs were also tested, and the Higuchi model was selected as the optimal model based on the high correlation coefficient (Table 2). Because the diffusion indexes (n) were in the range of 0.43−0.85, which indicates that the releases of N, P, and Fe were controlled by non-Fickian diffusion.[39] In addition, MOF1 benefited the rice production, that is, significantly increased the rice yield (Table 3) as well as the dry matter mass of straw (stem and leaf), nitrogen accumulation of rice grains, and nitrogen use efficiency (Table S3).

Table 2. Correlation Coefficients Obtained from Fitting Mathematical Models to the Release Data of N, P, and Fe from Fe-MOFs in Soil[a]

Fe-MOFs	models	R^2		
		N	P	Fe
MOF1	zero-order model	0.753	0.746	0.812
	first-order model	0.823	0.805	0.782
	Higuchi model	0.955 (n = 0.458)	0.962 (n = 0.492)	0.969 (n = 0.571)
	Ritger−Peppas model	0.892	0.935	0.917
MOF2	zero-order model	0.762	0.767	0.793
	first-order model	0.799	0.821	0.807
	Higuchi model	0.942 (n = 0.446)	0.951 (n = 0.476)	0.975 (n = 0.618)
	Ritger−Peppas model	0.881	0.912	0.906

[a] n, diffusion indexes.

Degradation of Fe-MOFs in Soil. The degradation rates were studied by weighing. Within 98 days, the degradation rates of MOF 1 and MOF2 were 82 and 72%, respectively (Figure S2). In the presence of soil, the MOF structure changed significantly. On the 7th day of culture, cracks and faults appeared on both MOF surfaces. Over time, the MOF surfaces gradually corroded and decomposed into smaller massive structures (Figure 7A,B). The infrared spectra showed a gradual decrease in characteristic MOF peak intensities, indicating a chemical structure change upon degradation (Figure 7C,D). At the same time, the characteristic peaks in the MOF LIBS spectra also decreased gradually with time, indicating that the MOF elements decrease gradually with degradation (Figure S3). The PXRD of MOFs showed that all diffraction peaks gradually weaken and some peaks disappear (Figure S4). In addition, decreases in the crystallinities of MOF1 and MOF2 were also found through calculations.

The organic ligand in this study was oxalic acid, and it played an important role in the soil ecosystem. It is reported that oxalate increases the available phosphorus in soil.[40,41] Oxalate−carbonate pathway is considered to be an important part of the geochemical carbon cycle. Its essence is the conversion of oxalate to carbonate (usually the biological conversion of calcium oxalate to calcium carbonate). However, due to the high activation energy required for oxalate oxidation, conversion of oxalate to carbonate does not occur spontaneously, though microorganisms use oxalate to drive this pathway. These bacteria use oxalate as a carbon source and energy. The enriched soil solution was inoculated on the agar plate modified by calcium oxalate. Due to the low solubility of calcium oxalate, the appearance of agar was opaque. Therefore, transparent areas around the calcium oxalate particles indicated the consumption of calcium oxalate by bacteria growing on agar, which further proved the existence of oxalate-consuming bacteria in the soil.[42] Therefore, these bacteria might cause MOF degradation by consuming oxalate (Figure 8).

A comparison of the structures of both MOFs revealed differences and similarities. Despite scaling the pilot synthesis up based on laboratory results, the flow, mass transfer, heat transfer, and other factors may change; this may alter crystal nuclei formation and/or crystal structures. However, the nutrient release behaviors of MOF1 and MOF2 were consistent, so both have potential for use as controlled-release fertilizers. Although researchers have made significant progress in MOF research recently, very little has seen industrial or commercial adaptation.[43] Different from laboratory-scale studies, the industrial production of MOF materials must consider production applicability, production cost, and treatment of "three wastes" (waste gases, wastewater, and waste residues). The hydrothermal process utilized in this pilot plant study was mild and controllable, but the yields were relatively low (<30%). Therefore, recovering the metal ions and organic ligands in the solution, realizing the continuous and efficient synthesis of MOFs, and improving the MOF yields represent the next steps in this important area. Although many other factors require consideration and solving for the industrial production of MOF controlled-release fertilizers, the overall

https://doi.org/10.1021/acsomega.2c05093
ACS Omega 2022, 7, 35970−35980

Table 3. Effects of Fe-MOFs Synthesized in the Pilot Scale on the Yield and Agronomic Traits of Rice[a]

agronomic traits	CK	CF	Fe-MOFs
yields ($kg \cdot hm^{-2}$)	5490 ± 463 b	10231.5 ± 1426 a	10429.5 ± 1022 a
1000 kernel weight (g)	32.66 ± 0.56 a	32.24 ± 0.36 a	31.80 ± 0.35 a
number of kernels per ear	71.58 ± 8.78 b	92.25 ± 5.41 a	94.25 ± 2.17 a
effective ear number ($\times 10^6 \cdot hm^{-2}$)	7.67 ± 0.67 b	11.44 ± 0.38 a	10.17 ± 0.38 a
seed-setting rate (%)	95.28 ± 0.73 a	95.17 ± 0.33 a	95.74 ± 0.37 a

[a]CK—no fertilizer control; CF—conventional fertilizer; values followed by different small letters in the same line mean significant difference among treatments ($p < 0.05$).

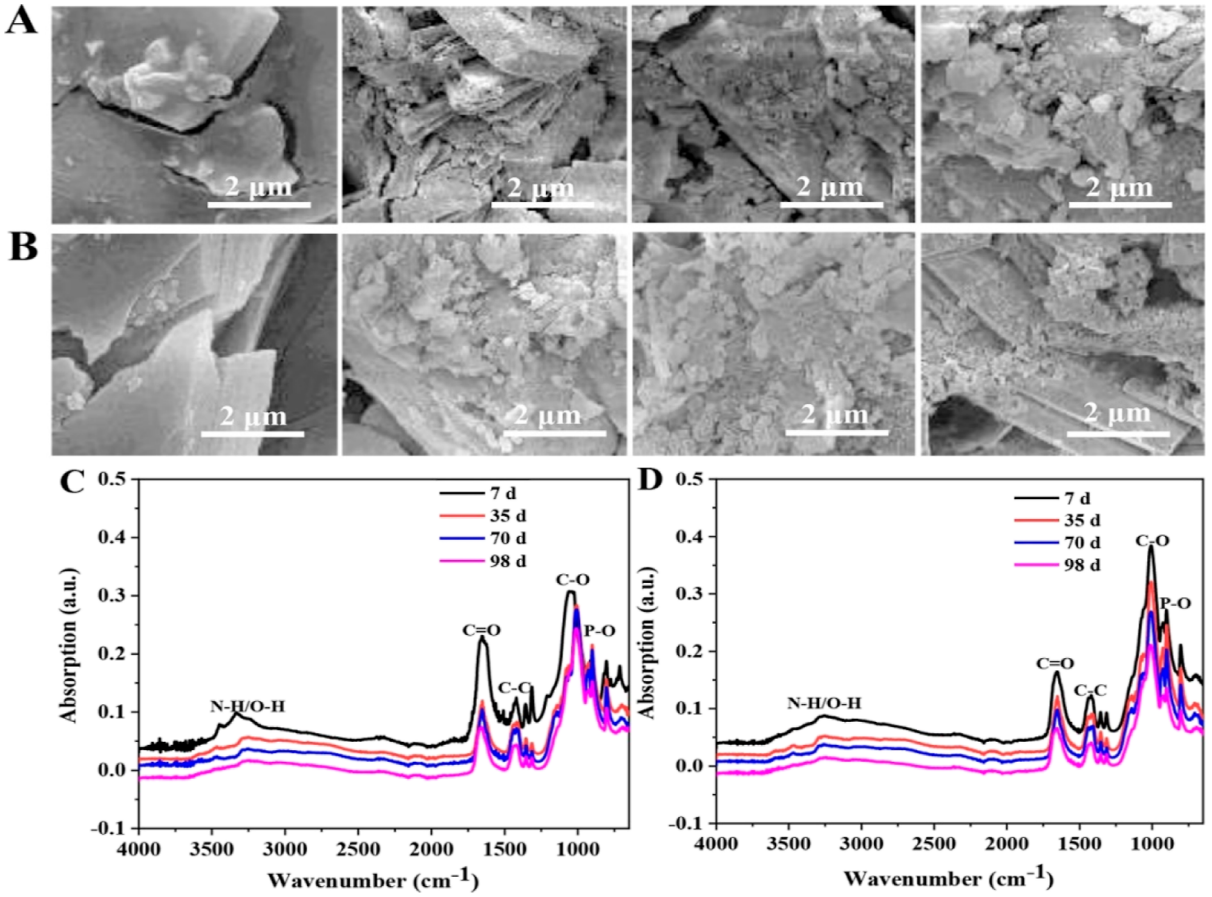

Figure 7. Degradation of Fe-MOFs in soil. SEM images of MOF1 (A) and MOF2 (B) at different degradation times. FTIR-ATR spectra of MOF1 (C) and MOF2 (D) at different degradation times.

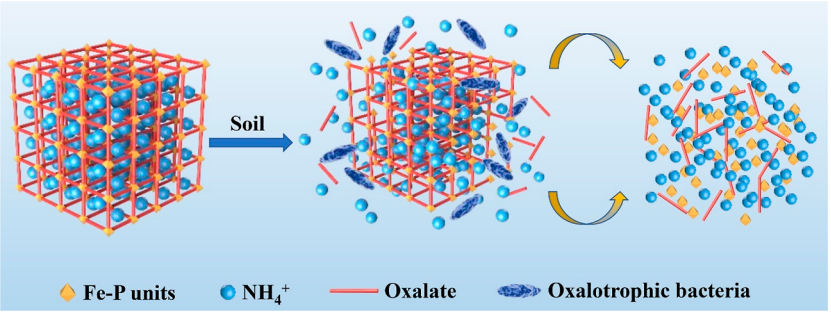

Figure 8. Schematic diagram of MOF degradation.

synthetic process developed in this study provides a foundation for additional studies to support the production of next generation of industrial MOF materials.

CONCLUSIONS

Under hydrothermal reaction conditions, we developed a pilot-scale preparation of a new Fe-MOF rich in nitrogen, phosphorus, and iron nutrients. FTIR, LIBS, XPS, and

https://doi.org/10.1021/acsomega.2c05093
ACS Omega 2022, 7, 35970−35980

SEM−EDX characterizations showed that all substrates were involved in the Fe-MOF synthesis. The Fe-MOFs had a chemical structure similar to the laboratory-synthesized Fe-MOFs with the molecular formula of $C_2H_{15}Fe_2N_2O_{18}P_3$. The Fe-MOFs showed better nutrient release behavior in soil than that in water, which matched well with the crop growth, thereby effectively improving nitrogen use efficiency, agronomic indicators, and crop yield. As a result, the Fe-MOFs had the potential for use as a controlled-release fertilizer. The successful pilot-scale synthesis of Fe-MOFs confirmed the feasibility of the synthetic process, provided reference and support for the industrial production of Fe-MOFs as a new controlled-release fertilizer in the future, and provided novel ideas for the development of new fertilizers.

■ ASSOCIATED CONTENT

Supporting Information

The Supporting Information is available free of charge at https://pubs.acs.org/doi/10.1021/acsomega.2c05093.

Experimental characterizations including PXRD, LIBS, and single-crystallographic data; degradation rates of Fe-MOFs; and the effects of Fe-MOFs on rice (PDF)

■ AUTHOR INFORMATION

Corresponding Author

Changwen Du − *The State Key Laboratory of Soil and Sustainable Agriculture, Institute of Soil Science Chinese Academy of Sciences, Nanjing 210008, China; College of Advanced Agricultural Sciences, University of Chinese Academy of Sciences, Beijing 100049, China;* orcid.org/0000-0002-9064-3581; Phone: +86-25-86881565; Email: chwdu@issas.ac.cn

Authors

Ke Wu − *The State Key Laboratory of Soil and Sustainable Agriculture, Institute of Soil Science Chinese Academy of Sciences, Nanjing 210008, China; College of Environment and Ecology, Jiangsu Open University, Nanjing 210017, China*

Xuebin Xu − *The State Key Laboratory of Soil and Sustainable Agriculture, Institute of Soil Science Chinese Academy of Sciences, Nanjing 210008, China*

Fei Ma − *The State Key Laboratory of Soil and Sustainable Agriculture, Institute of Soil Science Chinese Academy of Sciences, Nanjing 210008, China*

Complete contact information is available at: https://pubs.acs.org/10.1021/acsomega.2c05093

Notes

The authors declare no competing financial interest.

■ ACKNOWLEDGMENTS

This work was supported by the Strategic Priority Research Program of the Chinese Academy of Sciences (XDA28120400) and the National Natural Scienc Foundation of China (32202613).

■ ABBREVIATIONS

MOFs, metal−organic frameworks; Fe-MOFs, iron-based metal−organic frameworks; FTIR-ATR, Fourier transform infrared attenuated total reflectance spectrocopy; FTIR-PAS, Fourier transform infrared photoacoustic spectroscopy; LIBS, laser-induced breakdown spectroscopy; XPS, X-ray photoelectron spectroscopy; ICP-OES, inductively coupled plasma optical emission spectrometry; XRD, X-ray diffraction; SEM, scanning electron microscopy; EDX, energy-dispersive X-ray spectroscopy

■ REFERENCES

(1) Naz, M. Y.; Sulaiman, S. A. Slow release coating remedy for nitrogen loss from conventional urea: a review. *J. Controlled Release* **2016**, *225*, 109−120.

(2) Yang, Y.; Zhang, M.; Li, Y.; Fan, X.; Geng, Y. Improving the quality of polymer coated urea with recycled plastic, properadditives, and large tablets. *J. Agric. Food Chem.* **2012**, *60*, 11229−11237.

(3) Katsumi, N.; Kusube, T.; Nagao, S.; Okochi, H. Accumulation of microcapsules derived from coated fertilizer in paddy fields. *Chemosphere* **2021**, *267*, 129185.

(4) Qiao, D.; Liu, H.; Yu, L.; Bao, X.; Simon, E.; Petinakis, L.; Chen, L. Preparation and characterization of slow-release fertilizer encapsulated by starch-based superabsorbent polymer. *Carbohydr. Polym.* **2016**, *147*, 146−154.

(5) Wang, X.; Lü, S.; Gao, C.; Feng, C.; Xu, X.; Bai, X.; Gao, N.; Yang, J.; Liu, M.; Wu, L. Recovery of Ammonium and phosphate from waste water by wheat straw based amphoteric adsorbent andreusing as a multifunctional slow release compound fertilizer. *ACS Sustainable Chem. Eng.* **2016**, *4*, 2068−2079.

(6) Xie, L.; Liu, M.; Ni, B.; Wang, Y. Utilization of wheat straw forthe preparation of coated controlled-release fertilizer with the function of water retention. *J. Agric. Food Chem.* **2012**, *60*, 6921−6928.

(7) Wang, X.; Lü, S.; Gao, C.; Xu, X.; Wei, Y.; Bai, X.; Feng, C.; Gao, N.; Liu, M.; Wu, L. Biomass based multifunctional fertilizer system featuring controlled release nutrient, water retention andamelioration of soil. *RSC Adv.* **2014**, *4*, 18382−18390.

(8) Ni, B.; Liu, M.; Lü, S.; Xie, Y.; Wang, Y. Environmentally friendly slow release nitrogen fertilizer. *J. Agric. Food Chem.* **2011**, *59*, 10169−10175.

(9) Farha, O. K.; Eryazici, I.; Jeong, N. C.; Hauser, B. G.; Wilmer, C. E.; Sarjeant, A. A.; Snurr, R. Q.; Nguyen, S. T.; Yazaydın, A. O.; Hupp, J. T. Metal organic framework materials with ultra high surface areas: is the sky the limit? *J. Am. Chem. Soc.* **2012**, *134*, 15016−15021.

(10) Noro, S.; Mizutani, J.; Hijikata, Y.; Matsuda, R.; Sato, H.; Kitagawa, S.; Sugimoto, K.; Inubushi, Y.; Kubo, K.; Nakamura, T. Porous coordination polymers with ubiquitous and biocompatible metals and a neutral bridging legend. *Nat. Commun.* **2015**, *6*, 5851−5859.

(11) Stock, N.; Biswas, S. Synthesis of the metal-organic frameworks (MOFs): routes to various MOF topologies, morphologies, andcomposites. *Chem. Rev.* **2012**, *112*, 933−969.

(12) Zhao, Y.; Kornienko, N.; Liu, Z.; Zhu, C.; Asahina, S.; Kuo, T. R.; Bao, W.; Xie, C.; Hexemer, A.; Terasaki, O.; Yang, P.; Yaghi, O. M. Mesoscopic constructs of ordered and oriented metal organic frameworks on plasmonic silver nanocrystals. *J. Am. Chem. Soc.* **2015**, *137*, 2199−2202.

(13) Kitagawa, S.; Kitaura, R.; Noro, S. Functional porous coordination polymers. *Angew. Chem., Int. Ed. Engl.* **2004**, *43*, 2334−2375.

(14) Suh, M. P.; Park, H. J.; Prasad, T. K.; Lim, D. Hydrogen storage in metal organic frameworks. *Chem. Rev.* **2012**, *112*, 782−835.

(15) Farrusseng, D.; Aguado, S.; Pinel, C. Metal-organic frameworks: Opportunities for catalysis. *Angew. Chem., Int. Ed. Engl.* **2009**, *48*, 7502−7513.

(16) Dang, S.; Ma, E.; Sun, Z.; Zhang, H. A layer-structured Eu-MOF as a highly selective fluorescent probe for Fe^{3+} detection through a cation-exchange approach. *J. Mater. Chem.* **2012**, *22*, 16920−16926.

(17) Hao, J.; Yan, B. A water-stable lanthanide functionalized MOF as ahighly selective and sensitive fluorescent probe for Cd^{2+}. *Chem. Commun.* **2015**, *51*, 7737−7740.

(18) Lv, R.; Chen, Z.; Fu, X.; Yang, B.; Li, H.; Su, J.; Gu, W.; Liu, X. A highly selective and fast-response fluorescent probe based on Cd-MOF for the visual detection of Al^{3+} ion and quantitative detection of Fe^{3+} ion. *J. Solid State Chem.* **2018**, *259*, 67−72.
(19) McKinlay, A. C.; Morris, R. E.; Horcajada, P.; Férey, G.; Gref, R.; Couvreur, P.; Serre, C. *Angew. Chem., Int. Ed.* **2010**, *49*, 6260−6266.
(20) Abdelhameed, R. M.; Abdelhameed, R. E.; Kamel, H. A. Iron-based metal organic frameworks as fertilizers for hydroponically grown Phaseolus vulgaris. *Mater. Lett.* **2019**, *237*, 72−79.
(21) Anstoetz, M.; Rose, M. W.; Clark, L. H.; Yee, C. A.; Raymond, T.; Vancov, T. Novel applications foroxalate-phosphate-amine metal organic frameworks (OPA-MOFs): Can an iron-based opa-mof be used asslow-release fertilizer? *PLoS One* **2015**, *10*, No. e0144169.
(22) Wu, K.; Du, C.; Ma, F.; Shen, Y.; Zhou, J. Optimization of metal organic (citric acid) frameworks for controlled release of nutrients. *RSC Adv.* **2019**, *9*, 32270−32277.
(23) Du, Y.; Xu, X.; Ma, F.; Du, C. Solvent free synthesis of iron based metal organic frameworks (MOFs) as slow-release fertilizers. *Polymers* **2021**, *13*, 561.
(24) Cao, Y.; Huang, L.; Chen, J.; Liang, J.; Long, S.; Lu, Y. Development of a controlled release formulation based on a starch matrix system. *Int. J. Pharm.* **2005**, *298*, 108−116.
(25) Chen, C.; Zhang, G.; Dai, Z.; Xiang, Y.; Liu, B.; Bian, P.; Zheng, K.; Wu, Z.; Cai, D. Fabrication of light-responsively controlled-release herbicide using a nanocomposite. *Chem. Eng. J.* **2018**, *349*, 101−110.
(26) Huang, G.; Deng, Y.; Zhang, Y.; Feng, P.; Xu, C.; Fu, L.; Lin, B. Study on long-term pest control and stability of double-layer pesticide carrier in indoor and outdoor environment. *Chem. Eng. J.* **2021**, *403*, 126342.
(27) Siepmann, J.; Peppas, N. A. Higuchi equation: derivation, applications, use and misuse. *Int. J. Pharm.* **2011**, *418*, 6−12.
(28) Jiang, Y.; Wang, S. L.; Lii, K. H.; Nguyen, N.; Ducouret, A. Synthesis, Crystal Structure, Magnetic Susceptibility, and Mössbauer Spectroscopy of a Mixed-Valence Organic−Inorganic Hybrid Compound: (H3DETA)[Fe3(C2O4)2(HPO4)2(PO4)] (DETA = Diethylenetriamine). *Chem. Mater.* **2003**, *15*, 1633−1638.
(29) DeBord, J. R. D.; Reiff, W. M.; Warren, C. J.; Haushalter, R. C.; Zubieta, J. A 3-D organically templated mixed valence (Fe^{2+}/Fe^{3+}) iron phosphate with oxide-centered $Fe_4O(PO_4)_4$ cubes: hydrothermal synthesis, crystal structure, magnetic susceptibility, and mössbauer spectroscopy of $[H_3NCH_2CH_2NH_3]_2[Fe_4O(PO_4)_4]\cdot H_2O$. *Chem. Mater.* **1997**, *9*, 1994−1998.
(30) Rajic, N.; Stojakovic, D. R.; Hanzel, D.; Kaucic, V. The structure directing role of 1,3-diaminopropane in the hydrothermal synthesis of iron (III) phosphate. *J. Serb. Chem. Soc.* **2004**, *69*, 179−186.
(31) Abu-Shandi, K.; Winkler, H.; Wu, B.; Janiak, C. Open-framework iron phosphates: Syntheses, structures, sorption studies and oxidation catalysis. *CrystEngComm* **2003**, *5*, 180−189.
(32) Sandineni, P.; Ghosh, K.; Choudhury, A. Electrochemistry of lllusive barbosalite, $Fe^{2+}Fe^{3+}{}_2(PO_4)_2(OH)_2$: an iron phosphate related to lipscombite structure. *J. Electrochem. Soc.* **2019**, *166*, A3585−A3592.
(33) Xie, J.; Yang, Y.; Gao, B.; Wan, Y.; Li, Y.; Cheng, D.; Xiao, T.; Li, K.; Fu, Y.; Xu, J.; Zhao, Q.; Zhang, Y.; Tang, Y.; Yao, Y.; Wang, Z.; Liu, L. Magnetic-Sensitive Nanoparticle Self-Assembled Super-hydrophobic Biopolymer-Coated Slow-Release Fertilizer: Fabrication, Enhanced Performance, and Mechanism. *ACS Nano* **2019**, *13*, 3320−3333.
(34) Xie, J.; Yang, Y.; Gao, B.; Wan, Y.; Li, Y.; Xu, J.; Zhao, Q. Biomimetic superhydrophobic biobased polyurethane-coated fertilizer with atmosphere "outerwear". *ACS Appl. Mater. Interfaces* **2017**, *9*, 15868−15879.
(35) Forster, P. M.; Cheetham, A. K. Hybrid inorganic−organic solids: an emerging class of nanoporous catalysts. *Top. Catal.* **2003**, *24*, 79−86.
(36) Stumm, W.; Morgan, J. J.*Aquatic Chemistry: Chemical Equilibria and Rates in Natural Waters*, 3rd edn; John Wiley and Sons, 1995.
(37) Cailleau, G.; Braissant, O.; Dupraz, C.; Aragno, M.; Verrecchia, E. P. Biologically induced accumulations of $CaCO_3$ in orthox soils of Biga, Ivory Coast. *Catena* **2005**, *59*, 1−17.
(38) Anstoetz, M.Synthesis Optimisation, Characterisation and Evaluation of an Iron-Based Oxalate-Phosphate-Amine MOF (OPA-MOF) for Innovative Application in Agriculture, Ph.D. Thesis, Southern Cross University, Lismore, NSW, Australia, 2016.
(39) Shen, Y.; Wang, H.; Liu, Z.; Li, W.; Liu, Y.; Li, J.; Wei, H.; Han, H. Fabrication of a water-retaining, slow-release fertilizer based on nanocomposite double-network hydrogels via ion-crosslinking and free radical polymerization. *J. Ind. Eng. Chem.* **2021**, *93*, 375−382.
(40) Braissant, O.; Cailleau, G.; Aragno, M.; Verrecchia, E. Biologically induced mineralization in the iroko Miliciaexcelsa (Moraceae): its causes and consequences to the environment. *Geobiology* **2004**, *2*, 59−66.
(41) Martin, G.; Guggiari, M.; Bravo, D.; Zopfi, J.; Cailleau, G.; Aragno, M.; Job, D.; Verrecchia, E.; Junier, P. Fungi, bacteria and soil pH: the oxalate-carbonate pathway as a model for metabolic interaction. *Environ. Microbiol.* **2012**, *14*, 2960−2970.
(42) Aragno, A.; Verrecchia, E. P.; Job, D.; Cailleau, G.; Braissant, O.; Khammar, N.; Ferro, K.; Mota, M.; Guggiari, M.; Martin, G. Calcium carbonate biomineralization in ferralitic, tropical soils through the oxalate-carbonate pathway. *BGS Bull.* **2010**, *30*, 127−130.
(43) Ren, J.; Dyosiba, X.; Musyoka, N. M.; Langmi, H. W.; Mathe, M.; Liao, S. Review on the current practices and efforts towards pilot-scale production of metal-organic frameworks (MOFs). *Coord. Chem. Rev.* **2019**, *352*, 187−219.

https://doi.org/10.1021/acsomega.2c05093
ACS Omega 2022, 7, 35970−35980